Journal of Microelectronics and Electronic Packaging (2008) **5**, 52-61
Copyright © International Microelectroelectronics And Packaging Society
ISSN: 1551-4897

Maximum Attainable Deflections of Shape Memory Alloy-Layered Microcantilever

P. Majumder and A. Bhattacharyya*

***Abstract*—Finite element modeling of a shape memory alloy (SMA)-layered microcantilever is reported herein. It is assumed that the SMA layer is "two-way–trained," such that alternate heating and cooling of the SMA layer will cause a phase transformation in the SMA layer and deform the cantilever out-of-plane and back. For a nickel–titanium (NiTi) layer on a glass substrate, computational results indicate that a uniform 4% two-way strain along the length of a SMA layer spanning the full length of a 100-μm cantilever translates to a tip deflection of 29.5 μm, and a sweep of approximately 30° from the flat "rest" state. As well, 40% of the cantilever surface (measured from its free end) is flat and can be used as a flat reflective surface for micromirror applications. A "worse-case" analysis is presented where only 50% of the SMA length is able to undergo phase transformation, resulting in deflections of about 10 μm with a 12° sweep. Finally, it is shown that deflections are about two orders of magnitude higher than what would be possible if the SMA layer did not undergo phase transformations (but underwent pure thermal expansion only). One possible area of application could be in the area of continuously rotating micromirrors, suitable for surveillance systems.**

***Keywords*—SMA, two-way training, microcantilever, micromirrors**

Introduction

Two important applications of micromirrors are in the area of optical networks and light manipulation systems. In the former application, arrays of micromirrors are used as optical switches to transfer data from one optical cable to another in high-bandwidth telecommunication networks and also protect networks from disruptions. Two examples of currently available optical MEMS switches are the OMM optical switch from Optical Micromachines® [1] and the WaveStar™ LambdaRouter from Lucent Technologies. A more mature and highly successful application of micromirrors is the Digital Micromirror Device (DMD) of Texas Instruments [2] used for light modulation in digital projection systems. The actuation mechanism for the micromirrors in both applications is by electrostatic fields. A microcapacitor associated with each micromirror in the optical switch array enables the electrostatic actuation of the mirrors. In the DMD, each micromirror in the array corresponds to a pixel of the image. Actuation of each mirror is based on a digital signal, which activates a tiny electrode beneath each micromirror, causing it to tilt either toward or away from the light source. This leads to a complex actuation mechanism associated with each micromirror. The tilt is only ±10° from the reference plane [3]. In both applications, the electrostatic actuation precludes the micromirror from positioning itself at any other intermediate location between the "on" and "off" states. However, the frequency of actuation can be of the order of thousands of hertz. Certain applications, e.g., continuous surveillance systems, may not require as high an actuation frequency but may require the micromirror to take any possible position between the "on" and "off" states. While gimbaled systems have been widely used in two-axis MEMS scanners, these take up space and reduce the fill factor [22]. Thermally actuated shape memory alloy-layered microcantilevers may form the basis for such an application.

Shape memory alloys are smart materials that undergo a solid-solid phase transformation due to a change in stress (σ) and/or temperature (T). They exhibit unique properties of pseudoelasticity and shape memory [4, 5, 6]. These materials can exist in two different crystalline states known as austenite (A) and martensite (M). A schematic of the stress-temperature dependence of the transformation is shown in Fig. 1. A phase transformation from martensite to austenite starts at the austenite start temperature, A_s, and finishes at the austenitic finish temperature, A_f (where $A_s < A_f$). On cooling from a high temperature at which the SMA is in the austenite state, the SMA undergoes a phase transformation into martensite. This transformation starts at the martensite start temperature, M_s (where $M_s < A_s$), and finishes at the martensitic finish temperature, M_f (where $M_s > M_f$).

Some of the macroscopic features of the phase transformation are described in the context of deformation of a SMA wire. Consider the wire to be subjected to cyclic heating and cooling under constant mechanical load. Using Fig. 2, the actuation of the wire is described. A SMA wire in the martensitic state at room temperature and *in absence of mechanical load* (position 1) transforms into the austenite phase (position 2) on heating. When the wire is cooled back to room temperature, it changes back to its original martensite state (position 1). The microstructural state at position 1 is referred to as "self-accommodated martensite," and macroscopically, there is negligible change in length between the austenite and martensite states. At this state, the martensite forms in different orientations (called "variants"), such that there is no overall deformation (except for thermal strains). However, if the wire at position 1 is subjected to a mechanical load, then the material goes to a detwinned martensite state (position 3). Detwinning is the process by which the different variants realign along the loading direction, leading to an observable

Manuscript received September 2007 and accepted May 2008
Smart Materials and MEMS Laboratory, Department of Applied Science, University of Arkansas at Little Rock, 2801 South University, Little Rock, Arkansas 72204
*Corresponding author; email: axbhattachar@ualr.edu

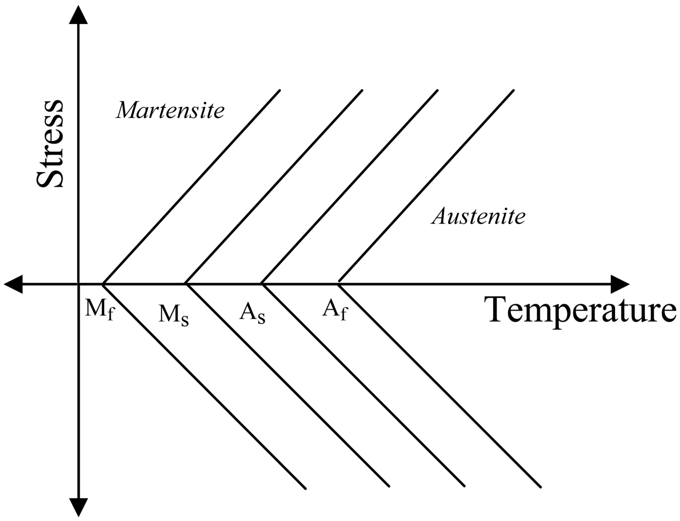

Fig. 1. Stress–temperature relationship of shape memory alloys.

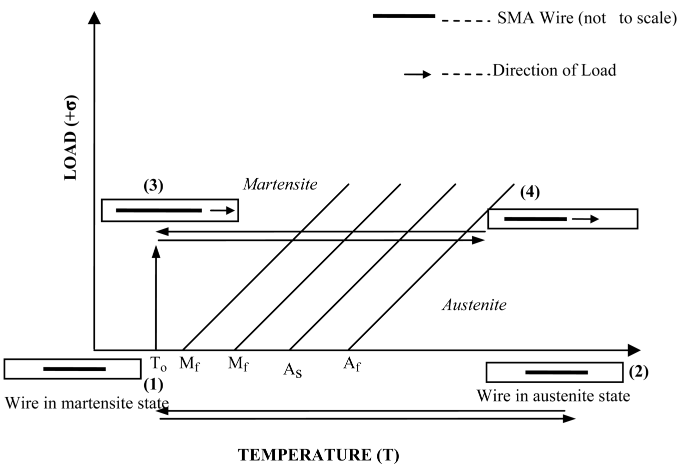

Fig. 2. Stress–temperature relationship for SMA wire "training."

change in length. At this state, the length of the wire is longer than what it was at position 1. If the wire is now heated to a temperature above A_f, then its phase changes to austenite at position 4, and a macroscopic decrease in length is observed. A commonly used commercially available SMA is the nickel–titanium (NiTi) alloy. A NiTi wire with a length of 10 cm and diameter of 0.254 mm can extend or actuate by about 1 cm when a mass of 2 kg is hung at one end (strain of ~10%). Heating the wire through ~30-40°C can reverse this length change. This is known as the one-way shape memory effect. Thereafter, repeated cyclic cooling and heating "trains" the SMA wire to remember its longer length in the martensite phase and the shorter length in the austenite phase. Once the SMA is "trained" and the load is removed such that the wire is back at position 1, cyclic heating and cooling between positions 1 and 3 is accompanied by strains of the order of 4-5%, regardless of an external load being applied or not [7]. This is known as the "two-way" memory effect. Partial phase transformations, where the SMA is heated beyond A_s (and below A_f) and then cooled, are accompanied by a change that is a fraction of the maximum that is attainable.

SMA thin-film fabrication is a relatively new area of activity. One of the earliest reported works was fabrication of NiTi thin films by RF magnetron sputtering in 1994 [8]. More recent efforts have reported NiTi thin-film fabrication approaches using electron beam evaporation [9], heated target deposition [10], and robust cosputtering [11]. SMA thin films have been used in applications such as micropumps for biomedical applications [12], microbubbles for flow control around air foils [13], microgrippers [14], and in optical applications [15]. Gill and Karman [13] have utilized the stoichiometric two-way memory effect in NiTi thin films for microbubble actuation. A significant challenge in fabricating SMA thin films is to ensure uniform stoichiometry. This is crucial because the transformation temperatures are highly sensitive to the stoichiometry [10]. The disadvantage of the electron beam evaporation method is that in this process it is difficult to maintain the uniformity of the film composition [9]. The heated target deposition technique [10] is much less controllable than the cosputtering method. The cosputtering technique permits control of the Ti sputter rate by adjusting the power input [11] in contrast to the heated target method, which relies upon the temperature of the target. This is not a reliable parameter as it is difficult to predict the temperature to be used and whether that temperature will produce efficient and repeatable results. To the best of our knowledge, the mechanically induced two-way memory effect in SMA thin film-based devices using a nonintrusive, external, electromagnetic approach has not yet been reported in the open literature. Although numerical experimentation is no substitute for actual experiments, it does offer a preliminary assessment of the performance of the aforementioned device before fabrication and characterization are attempted.

In this work, we report the finite element analysis of the steady-state deflections of a SMA thin-film–layered microcantilever for a given two-way phase transformation strain in the SMA layer. The analysis is carried out using the commercial finite-element software ABAQUS™. An approximate but simple method of assigning an average coefficient of thermal expansion for the SMA that captures thermal expansion as well as phase transformation is used. The effects of the phase transformation strain, the length of the SMA layer on the microcantilever, and partially transformed SMA layers are studied. This paper is organized into four sections. In the next section, we describe the SMA-actuated micromirror, a SMA constitutive model and the current approach. Finite-element modeling and the results obtained using this method, are presented in the section "Finite Element Method and Results." Finally, the conclusions, limitations, and the future work are discussed in the section "Conclusions, Limitations, and Future Work."

SMA-Layered Micromirror, SMA Constitutive Model, and Current Approach

A. SMA-Layered Micromirror

A two-way–trained SMA-layered cantilever is depicted in Fig. 3; the two-way training approach is described in the Appendix. The two-way–trained cantilever is in the martensitic "flat" state at room temperature and is expected to change to a high-temperature austenitic "deflected" state on heating (and vice versa). Thus, electrical heating of the SMA layer may be used to

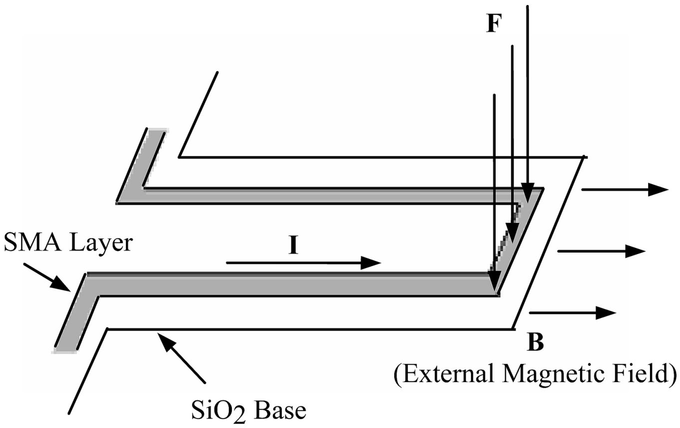

Fig. 3. SMA-layered microcantilever beam.

activate the two-way memory effect to bend the microcantilever. The cyclic increase and decrease in temperature due to electrical heating and subsequent cooling, respectively, will allow the SMA to switch between the austenite and martensite phase. Partial phase transformation by appropriate control of the thermal actuation will allow the microcantilever to take any position between the "rest" state and the fully actuated state. If the cantilever is coated with a reflective material, it can act as a mirror that can be actuated to take two extreme positions (the rest state and the fully deflected state) as well as the intermediate states in between. Modeling of the actuation of the SMA-layered cantilever will take the two-way–trained cantilever as its starting point and then determine the steady-state deflections of the cantilever when the SMA is heated. In the next section, we summarize the constitutive model based on which finite element computations are implemented.

B. SMA Constitutive Model

Research on constitutive models for SMAs is mature, with a wide variety of contributions in the literature [16]. In particular, the 3-D thermodynamic phenomenological constitutive model for SMAs as proposed by Boyd and Lagoudas [17] is suitable for engineering applications. Lagoudas and co-workers have developed their model to a high degree of sophistication. We shall recapitulate the 1-D version of the model that they first proposed in 1996 [17]. The crux of their model is the definition of an internal state variable, ξ, that represents the volume fraction of martensite at a given location in the SMA. The parameter, ξ, can take any value in the range $0 \leq \xi \leq 1$, where $\xi = 0$ corresponds to a fully austenitic state and $\xi = 1$ corresponds to a fully martensitic state. A crucial feature of this model, as of any other model for SMAs, is to propose an evolution equation that defines how ξ will evolve with stress, σ, and temperature, T. The evolution equation for a one-dimensional (1D) state of stress is given as [17]:

$$\xi = \frac{T - M_s^0}{(M_f^0 - M_s^0)} - \frac{\sigma}{D(M_f^0 - M_s^0)}, \qquad \text{A} \rightarrow \text{M transformation} \tag{1a}$$

$$\xi = \frac{T - A_f^0}{(A_s^0 - A_f^0)} - \frac{\sigma}{D(A_s^0 - A_f^0)}, \qquad \text{M} \rightarrow \text{A transformation} \tag{1b}$$

where the parameters M_s^0 and M_f^0 are the stress-free start and finish temperatures of the A → M transformation ($M_f^0 < M_s^0$), respectively, and A_s^0 and A_f^0 are the start and finish temperatures of the M → A transformation ($A_s^0 < A_f^0$), respectively. Due to the significant hysteresis in SMAs, the temperature range, $M_f^0 - M_s^0$, does not usually coincide with $A_s^0 - A_f^0$. The parameter D represents the stress needed to shift the transformation temperatures by 1°C.

The 1-D stress–strain relationship of the SMA in its rate form (i.e., with respect to time) is given as

$$\dot{\varepsilon} = \frac{1}{E(\xi)}\,\dot{\sigma} + \alpha\,(\xi)\,\dot{T} + \text{H}\dot{\xi}, \tag{2}$$

where ε is the strain, and the dot indicates the first derivative with respect to time; thus

$$\dot{\varepsilon} = \frac{\text{d}\varepsilon}{\text{d}t}$$

where t is time. The parameter, $E(\xi)$, is the martensite volume fraction-dependent Young's modulus of the SMA, $\alpha(\xi)$ is the coefficient of thermal expansion, and H is the maximum transformation strain ($H > 0$). The time derivatives of eqs. 1a and 1b can be inserted in eq. 2, resulting in

$$\dot{\varepsilon} = \frac{1}{E_{\text{eff}}}\,\dot{\sigma} + \alpha_{\text{eff}}\,\dot{T}, \tag{3}$$

where, for the A→M transformation

$$E_{\text{eff}} = E\left[1 - \frac{EH}{D(M_f^0 - M_s^0)}\right]^{-1}, \qquad \alpha_{\text{eff}} = \alpha + \frac{H}{(M_f^0 - M_s^0)}, \tag{4}$$

and for the M→A transformation

$$E_{\text{eff}} = E\left[1 - \frac{EH}{D(A_s^0 - A_f^0)}\right]^{-1}, \qquad \alpha_{\text{eff}} = \alpha + \frac{H}{(A_s^0 - A_f^0)}. \tag{5}$$

We shall refer to E_{eff} and α_{eff} as an effective Young's modulus and an effective coefficient of thermal expansion for the SMA, respectively. Note that the coefficient of thermal expansion, α, is always positive. However, because x < M_s^0 and $A_s^0 < A_f^0$, whereas $H > 0$, there is a distinct possibility that $\alpha_{\text{eff}} < 0$. This is usually the case with most SMAs. The effective thermal expansion coefficient captures the net effect of two different phenomena during phase transformation while undergoing a temperature increase (or decrease). During a temperature increase, the material increases in length due to thermal expansion, but there is an additional effect of a decrease in length due to the phase change from martensite to austenite (and vice versa with a temperature decrease). The finite element calculations in this paper rely on the definition of the effective thermal expansion coefficient, as defined in eq. 5.

C. Current Approach

The finite element calculations in this paper focus on determination of the deflected state of the cantilever at steady state after the SMA layer has been heated using a heat source. The steady-state option in the finite element code simply calculates

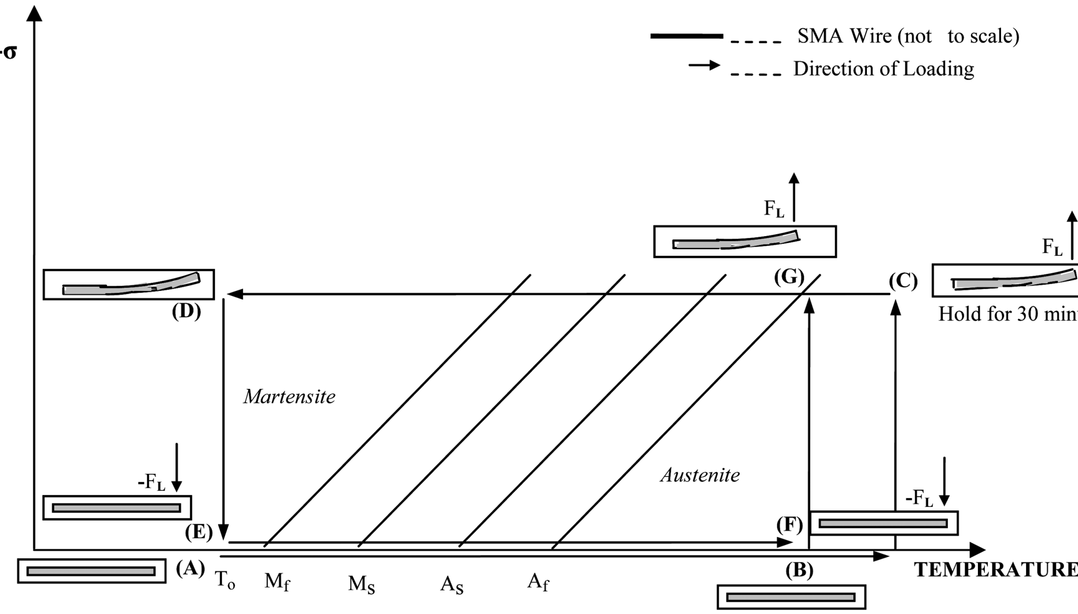

Fig. 4. Stress–temperature relationship for SMA-layered microcantilever "training."

the steady-state temperatures once the thermal problems (heat sources/sinks, boundary conditions etc.) are specified. In order to capture the effect of the phase transformation as the SMA is heated from an ambient state to a given temperature, we define an "effective" thermal expansion coefficient, $\overline{\alpha}(T)$, over a temperature range, T_0 and T, as $\overline{\alpha}(T) =$

$$\overline{\alpha}(T) = \int_{T_0}^{T} \frac{\alpha_{\text{eff}}}{(T - T_0)}\, dT. \tag{6}$$

Then, using the second of eq. 5 and recognizing that $\alpha_{\text{eff}} = \alpha$ when $T < A_s^0$ and $T > A_f^0$, we have

$$\overline{\alpha}(T) = \begin{cases} \alpha, & T_0 \le T < A_s^0 \\ \dfrac{(A_s^0 - T_0)\,\alpha + (T - A_s^0\,\alpha_{\text{eff}}}{(T - T_0)}, & A_s^0 \le T < A_f^0 \\ \dfrac{\{(T - T_0) - (A_f^0 - A_s^0)\}\,\alpha + (A_f^0 - A_s^0)\,\alpha_{\text{eff}}}{(T - T_0)}, & T \le A_f^0 \end{cases} \tag{7}$$

Here $\overline{\alpha}(T)$ represents the value of the "effective" thermal expansion coefficient along only one direction. This direction will be associated with the length of the cantilever and will be referred to as $\overline{\alpha}_{11}(T)$. However, in SMAs, phase transformation is a volume-preserving phenomenon that occurs due to a shear strain [5]. If the SMA is an isotropic material, this implies that

$$H_{22} = -\frac{1}{2} H_{11} \quad \text{and} \quad H_{33} = -\frac{1}{2} H_{11} \tag{8}$$

(note that H_{11} is simply "H"). The corresponding $\overline{\alpha}_{22}(T)$ and $\overline{\alpha}_{33}(T)$ will follow from eq. 7 once the parameter H in α_{eff} (via eq. 5) is replaced by H_{22} and H_{33}, respectively.

Finite Element Method and Results

A. Geometric Model and Solution Approach

The SMA-actuated microcantilever is modeled using the commercial finite element code ABAQUS™. The specific geometry we have modeled is shown in Fig. 5. For the finite element meshing (see Fig. 6) of our specific problem, solid hexahedral elements have been chosen from the ABAQUS™/Standard solid-element library. Hexahedral elements provide good accuracy and have a better convergence rate. Analysis is carried out to the second order as second-order elements provide higher accuracy in ABAQUS™/Standard than do first-order elements for problems that do not involve complex contact conditions, impact, or severe element distortions. These capture the stress concentrations more effectively and are better for modeling geometric features. Finally, these are effective in bending-dominated problems, as is the case with the microcantilever deflections here. The element control applied is reduced integration. The reduced integration elements use a lower-order integration to form the element stiffness. This reduces the running time, especially for spatially three-dimensional problems. Second-order reduced integration generally yields more accurate results than the corresponding fully integrated elements. For the thermal actuation, the "coupled temperature displacement" is the analysis procedure chosen in the *STEP option as it really is a thermomechanical problem and "heat transfer" is selected for pure thermal analysis. The model is assembled using separate parts available in the *PART module. The material properties for the SMA as well as the beam are included in the *PROPERTY option. ABAQUS™ has the capability to accept temperature-dependent data, as were input for the coefficient of thermal expansion for the SMA.

In the finite element calculations, we have modeled a NiTi SMA layer on a silicon dioxide (SiO_2) substrate. As the transformation temperatures of a NiTi SMA are highly sensitive to

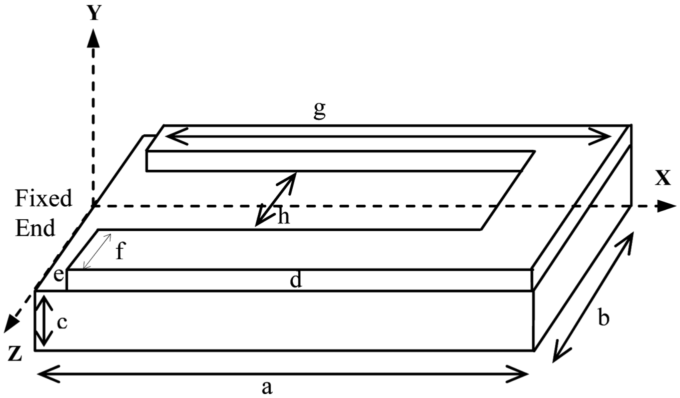

Fig. 5. Schematic view of SMA-layered microcantilever device.

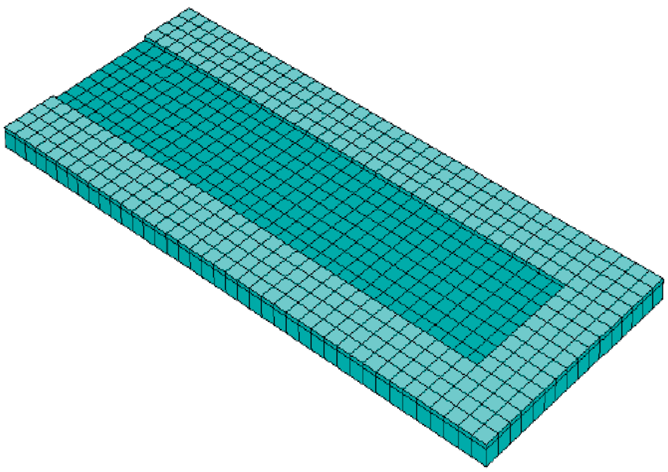

Fig. 6. Finite element meshing in ABAQUS™.

the alloy content [18], we have chosen $A_s^0 = 60°C$ and $A_f^0 = 90°C$. The phase transformation strain, H, has been taken to be 4% [7] along the length of the SMA layer. For information on all other material properties that we have used, please refer to Table I [19, 20]. We can now describe the mechanical and thermal boundary conditions. The left end of the beam is fixed (see Fig. 5). The interface between the SMA and the cantilever substrate is assumed to be mechanically and thermally perfect. As well, the left end of the beam is assumed to be at a constant ambient temperature of 25°C. Heat transfer from the surface of the cantilever is assumed to take place by free convection, the coefficient of which is taken as 6.6405×10^{-5} J mm^{-2} s^{-1} K^{-1} [21]. We have used a heat source of 0.8×10^{12} W m^{-3} in the SMA layer; this corresponds to an electrical current of 4.714 mA through the SMA layer. With these conditions, we have experimented with the geometric dimensions of the SMA-layered cantilever so as to reduce the stresses in the SMA to realistic levels and also attain high deflections. The geometric dimensions that we have used to obtain the results reported in Figs. 7-11 are summarized in Table II.

B. Steady-State Temperature Field

Fig. 8 shows the steady-state temperature distribution in the cantilever. As expected, temperatures increase along the length

Table I
Material Properties for the SiO_2 Substrate and the NiTi SMA actuator

Material	Young's modulus (GPa)	Poisson's ratio	Thermal conductivity (W m^{-1} °C^{-1})	Coefficient of thermal expansion
SiO_2 [20]	75	0.17	1.25	7×10^{-6} °C^{-1}
NiTi SMA [19]	50	0.33	13	Temperature-dependent

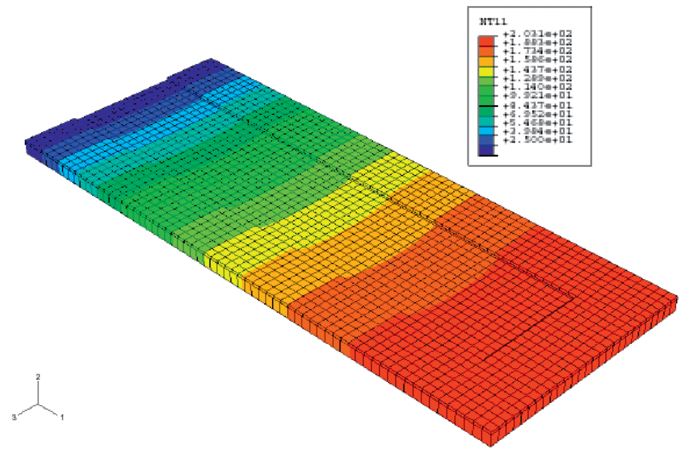

Fig. 7. Thermomechanical response of the SMA-layered cantilever with H_{11} = 4% and $H_{22} = H_{33} = -2\%$ with full phase transformation. Shown here are the (a) deflection, (b) stress, and (c) strain along the *x* axis upon thermal actuation as well as the contour distribution over the cantilever.

Table II
Device Dimensions (μm) as Indicated in Fig. 5

a	100	*e*	2.5
b	40	*f*	10
c	2	*g*	100
d	0.5	*h*	20

of the cantilever from the isothermal condition of room temperature (25°C). The maximum temperature attained is ~202.9°C. It can be clearly seen that almost 50% of the SMA layer is able to reach temperatures equal to or higher than A_s (at which the initial martensite state would start transforming to austenite). This is the portion of the SMA between 50 and 100 μm at the free end. Based on this estimation, two sets of results are given. In the first set, the entire SMA layer is taken to undergo a phase change. In the second set, the model is amended to capture the effects of partial phase transformations where only 50% of the SMA layer undergoes phase change. This is done by applying the phase transformation strain tensor to the SMA layer only between 50 and 100 μm at the free end. The layer between 0 (at the fixed end) and 50 μm is allowed to undergo pure thermal expansion only.

C. Mechanical Response of the Microcantilever

Figs. 8 and 9 pertain to the mechanical response of the "nonchipped" microcantilever; the "nonchipped" model is where we

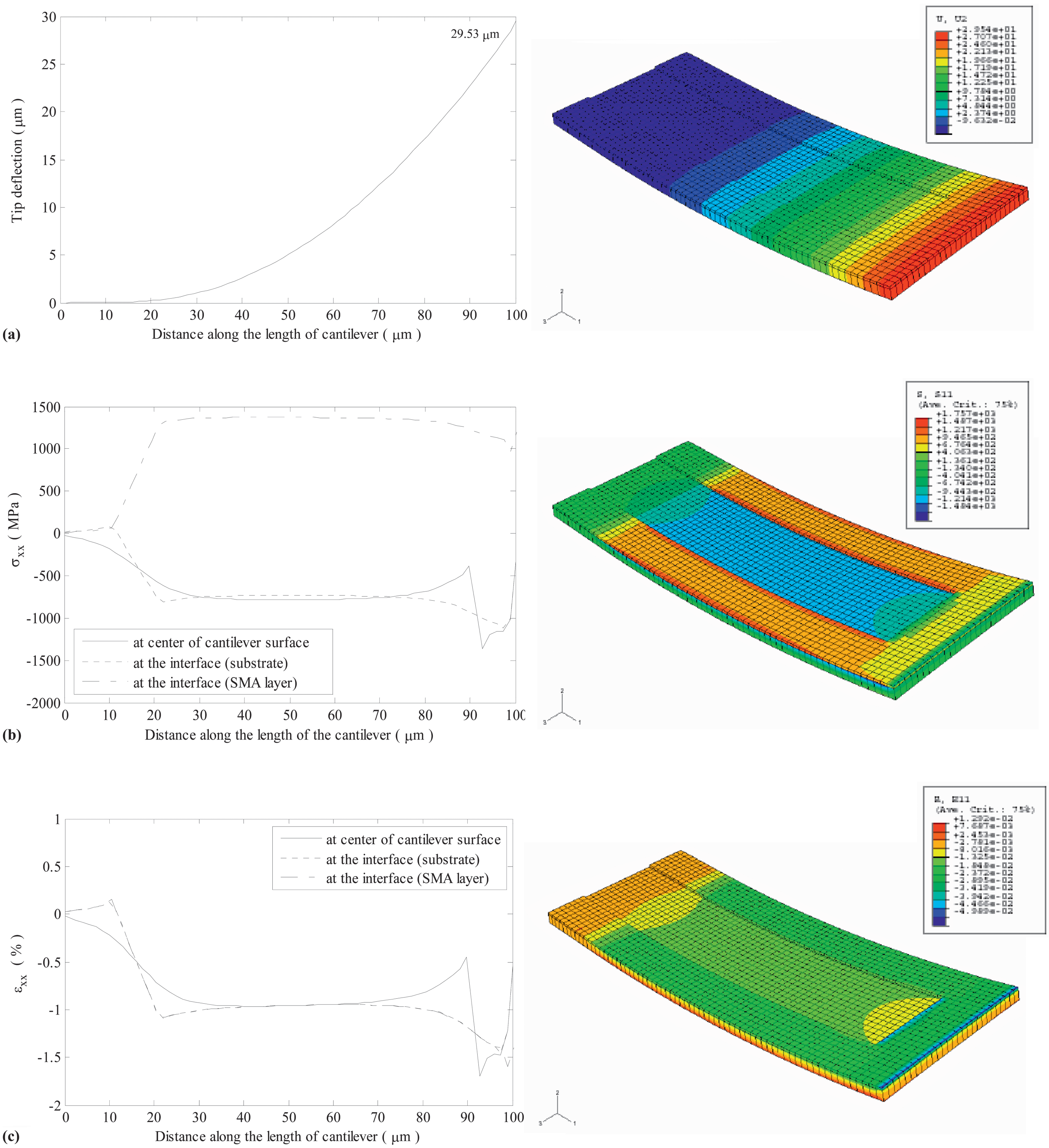

Fig. 8. Thermomechanical response of the SMA-layered cantilever with $H_{11} = 4\%$ and $H_{22} = H_{33} = -2\%$ with full phase transformation. Shown here are the (a) deflection, (b) stress, and (c) strain along x-axis upon thermal activation as well as the contour distribution over the cantilever.

take the parameter e in Fig. 5 as zero. In Fig. 8(a) is a plot of the vertical deflection of the top surface of the cantilever with respect to the x coordinate. Notice that the deflection at the tip is about 29.53 μm, and this corresponds to a sweep of approximately 30° from the flat “rest” state. Further for micromirror applications, it is desirable to have a significant portion of the cantilever surface to be flat (or without any curvature). It is also apparent that the region between 60 and 100 μm (measured from

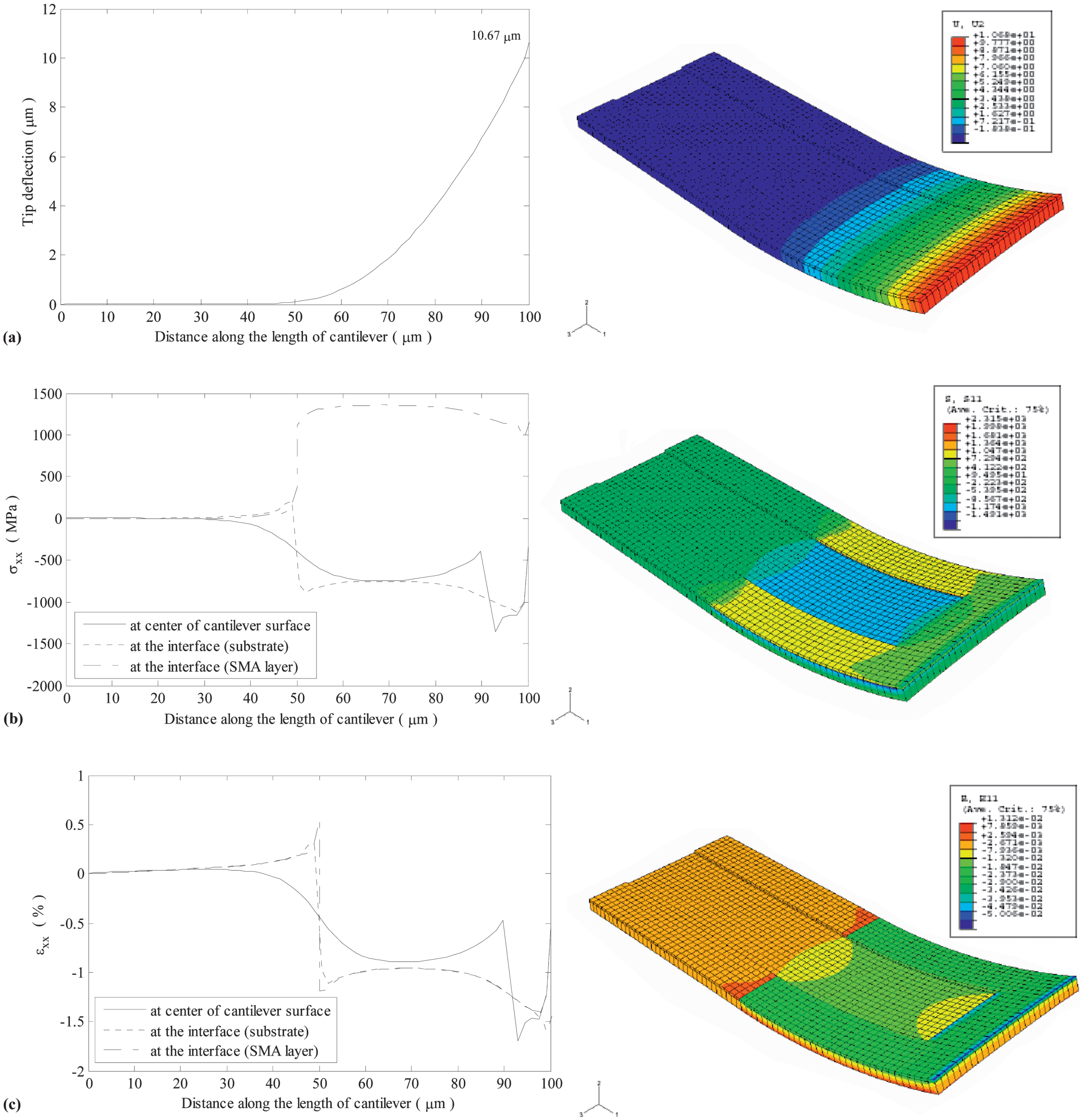

Fig. 9. Thermomechanical response of the SMA layered cantilever with $H_{11} = 4\%$ and $H_{22} = H_{33} = -2\%$ with partial phase transformation (in 50% length of SMA layer). Shown here are the (a) deflection, (b) stress, and (c) strain along the x axis upon thermal actuation as well as the contour distribution over the cantilever.

the left end) is reasonably flat (while having a mild curvature). Thus, almost 40% of the surface of the cantilever can be potentially used as a mirror surface. The stress along the x axis, σ_{xx}, is plotted with respect to the x coordinate in Fig. 8(b). The solid line represents the stress along the centerline of the top surface of the cantilever, while the two dashed lines show the stresses in the SMA and the substrate, both at the interface. Recall that the heating of the SMA layer results in a net contraction along the length of the cantilever. The compatibility requirement of a perfect interface between the SMA and its substrate translates into a tensile stress in the SMA layer and a compressive stress in the substrate (solid line). The stress in the substrate reaches a peak of about −1000 MPa (dotted line) at the interface of the cantilever with the SMA layer, whereas the stress in the SMA surface is positive (dashed–dotted line), also reaching a peak at about 1500 MPa. The contour plot of the stresses are also shown in Fig. 8(b). The distribution of the corresponding strain component, ε_{xx}, is shown in Fig. 8(c). Due to the compatibility requirement, the strains at the interface, both within the SMA and the substrate, are virtually identical. Because the substrate deformation in the substrate is purely thermoelastic, the stresses and strains in the substrate are of the same sign. On the other hand, the stresses in the SMA layer are predominantly tensile whereas the strains are compressive [compare Figs. 8(b) and (c)]. A more quantitative explanation can follow from eq. 2. This equation, in its total form after the martensite to austenite transformation is complete, can be written as in the second equation of eq. 9

$$\varepsilon_{xx} = E^{-1}\sigma_{xx} + \alpha(T - T_0) - H, \quad (9)$$
$$\sigma_{xx} = E(\varepsilon_{xx} + H - \alpha(T - T_0))$$

where, we recall, $H > 0$. The contractile nature of the phase transformation is captured by the term, $-H$, in the first of eq. 9. Rearranging this equation as in the second of eq. 9 and noting that the term $\alpha(T - T_0)$ is usually small compared with the rest of the terms in the parentheses, a negative (or compressive) ε_{xx} implies a positive σ_{xx} (as long as the magnitude of ε_{xx} is less than that of H).

Fig. 9 shows the steady-state thermomechanical response of the "nonchipped" model where only 50% of the SMA layer (from the free end and midway toward the fixed end) is allowed to undergo phase transformation. In Fig. 9(a), a plot of the vertical deflection of the top surface of the cantilever with respect to the x coordinate is shown. It can be observed that the deflection at the tip is only about 10.67 μm compared with the case when the entire SMA layer has undergone phase change and leads to a deflection of about 29.53 μm. This corresponds to a sweep of approximately 12° from the flat "rest" state versus the 30° sweep provided when the transformation happens in the complete layer. Almost 25% of the cantilever surface, i.e., the region between 75 and 100 μm (measured from the fixed end), is free of significant curvature. The stress component, σ_{xx}, along the length of the cantilever as well as the contour plot are shown in Fig. 9(b), whereas the strain component, ε_{xx}, is shown in Fig. 9(c). The trends in these quantities, while being confined primarily to the region where the phase transformation strain is operative, are otherwise qualitatively similar to those seen in Fig. 8.

In order to underscore the effect of the phase transformation, in Fig. 10 we have plotted log(deflection) with respect to the x coordinate, with and without phase transformation (the latter case follows from eq. 2 by setting $H = 0$). For both cases, the deflections of the "nonchipped" model and the "chipped" model (value of e is in Table II) have also been plotted. The maximum tip deflections for all four cases are indicated to the right of the figure. By comparing the results of the nonchipped model (second and fourth curves from the top), it is clear that the effect of the phase transformation results in cantilever deflections that are about two orders of magnitude higher than the deflections without the phase transformation; at the tip, deflection with phase transformation is 29.53 μm whereas deflection without phase transformation is 0.212 μm. This underscores the fact that, over a given temperature range, the occurrence of phase transformation, introduces a far higher sensitivity in the deflection of the

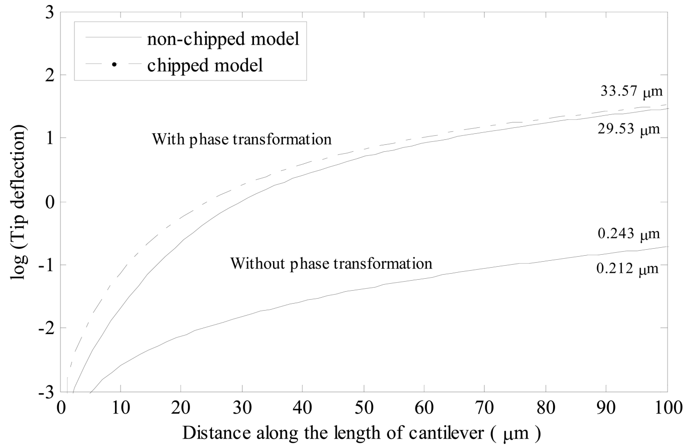

Fig. 10. Comparative study of the deflections of the SMA-layered microcantilever with ($H_{11} = 4\%$ and $H_{22} = H_{33} = -2\%$) and without phase transformation.

microcantilever to a temperature change as compared with the sensitivity that follows from pure thermal expansion. Similar trends are seen for the chipped model, with marginally higher values compared with the nonchipped model. Finally, Fig. 11 (for the nonchipped SMA model with full phase transformation of $H = 4\%$ in the entire SMA layer) shows that the tip deflection monotonically increases as the length of the SMA layer on the cantilever is increased. The minimum length of the SMA layer below which there is practically no deflection of the microcantilever is about 40 μm. It is also apparent that as the length of the SMA layer is increased from 40 to 70 μm, the tip deflection increases by about 23 μm. A further increase in length from 70 to 100 μm increases the microcantilever tip deflection only by about 7 μm. In closing, we recall the conservative assumption in setting H at 4%. Materials and device fabrication as well as innovative training procedures for the two-way actuation may permit higher strains and, thus, higher deflections of the microcantilever.

Conclusions, Limitations, and Future Work

A finite element model using the commercial finite element code, ABAQUS™, was developed to study the steady-state deflections of a thermally actuated SMA thin-film layered microcantilever. The model used the concept of an effective coefficient of thermal expansion approach to capture the nonlinear thermoelastic behavior of the shape memory alloys. For a nickel–titanium (NiTi) layer on a glass substrate, computational results indicate that a 4% two-way strain along the length of a SMA layer undergoing a volume-preserving phase transformation and spanning the full length of a 100-μm cantilever translates to a tip deflection of about 30 μm and a sweep of approximately 30° from the flat "rest" state. As well, 40% of the cantilever surface (measured from its free end) is reasonably flat, and may be used as a flat reflective surface for micromirror applications. Because the onset of phase change is highly dependent on the temperature distribution in the SMA layer with respect to the critical phase transformation temperatures (which also depends on the stresses in the SMA), a "worst-case" analysis is presented based on the pure thermal response of the cantilever. Here, only

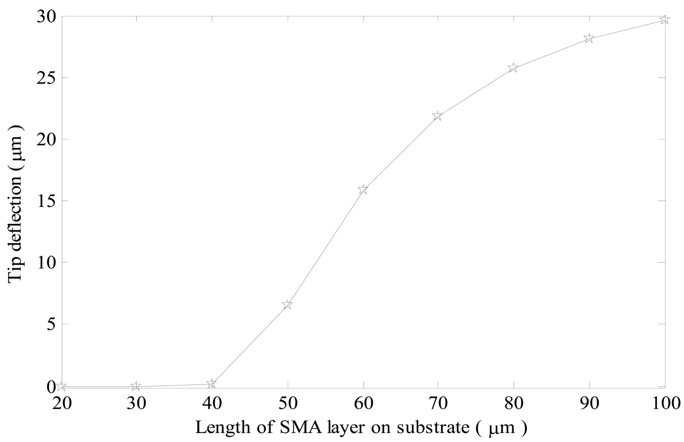

Fig. 11. Variation of tip deflection with change in the length of the SMA layer.

50% of the SMA length is allowed to transform, and this still results in deflections of about 10 μm with a 12° sweep. Finally, deflections are about two orders of magnitude higher than what it would be if the SMA layer did not undergo phase transformations (but did undergo pure thermal expansion only). One possible area of application could be in the area of continuously rotating micromirrors, suitable for surveillance systems. The future work will involve studying the transient response of the SMA-actuated cantilever and determining its frequency response.

Now we discuss two important assumptions: (i) The entire SMA layer need not necessarily have undergone the two-way training to an identical extent. Assuming otherwise is an approximation. It is possible that, during the training process, stresses at every location in the SMA layer may not have attained the critical value for the two-way training to occur. In addition, wherever the stresses do attain the critical value, there is no guarantee that the stress state would be identical in those locations. (ii) Recall the assumption made that the transformation temperatures are not dependent on the stresses. In context of these two assumptions, the results of the present work are primarily to be interpreted as the "maximum possible" deflection that may be attained by the cantilever. This, in other words, is the upper bound in the cantilever response. The lower bound of course can be computed by neglecting the two-way phase transformation during the thermal actuation of the SMA layer. We propose to address the limitations in future contributions.

References

[1] P.M. De Dobbelaere, S. Gloeckner, S.K. Patra, L. Fan, C. King, and K. Falta, "Design, manufacture, reliability of 2D MEMS optical switches", Proceedings of SPIE—The International Society for Optical Engineering, Vol. 4945, pp. 39-45, 2003.

[2] L.J. Hornbeck, "Digital light processing for high-brightness, high-resolution applications", Proceedings of SPIE—The International Society for Optical Engineering, Vol. 3013, pp. 27-40, 1997.

[3] J.B. Sampsell, "An overview of Texas Instruments Digital Micromirror Device (DMD) and its application to projection displays", Society for Information Display International Symposium, Digest of Technical Papers, Vol. 24, pp. 1012-1015, 1993.

[4] L.M. Schetky, "Shape memory alloys", Scientific American, Vol. 241, No. 5, pp. 74-82, 1979.

[5] V. Birman, "Review of mechanics of shape memory alloy structures", ASME Applied Mechanical Reviews, Vol. 50, No. 11, pp. 629-645, 1997.

[6] J.V. Humbeeck, "Shape memory alloys: a material and a technology", Advanced Engineering Materials, Vol. 3, pp. 837-850, 2001.

[7] D.A. Hebda and S.R. White, "Effect of training conditions and extended thermal cycling on nitinol two-way shape memory behavior", Smart Materials and Structures, Vol. 4, pp. 298-304, 1995.

[8] K. Nomura and S. Miyazaki, "The stability of shape memory characteristics against cyclic deformation in Ti–Ni sputter-deposited thin films", Proceedings of SPIE—The International Society for Optical Engineering, pp. 149-155, 1995.

[9] H.Y. Noh, K.H. Lee, X.X. Cui, and C-S. Choi, "The composition and structure of TiNi thin film formed by electron beam evaporation", Scripta Materialia, Vol. 43, No. 9, pp. 847-852, 2000.

[10] K.K. Ho and G.P. Carman, "Sputter deposition of NiTi thin film shape memory alloy using a heated target", Thin Solid Films, Vol. 370, pp. 18-29, 2000.

[11] C-L. Shih, B-K. Lai, H. Kahn, and S.M. Phillips, "A robust co-sputtering fabrication procedure for TiNi shape memory alloys for MEMS", IEEE Journal of Microelectromechanical Systems, Vol. 10, No. 1, pp. 69-79, 2001.

[12] W.L. Bernard, H. Kahn, A.H. Heuer, and M.A. Huff, "Thin film shape memory alloy-actuated micropumps", Journal of Microelectromechanical Systems, Vol. 7, pp. 245-251, 1998.

[13] J. Gill and G.P. Carman, "Three dimensional thin film shape memory alloy microactuator with inherent two-way actuation", Journal of Microelectromechanical Systems, Vol. 11, No. 1, pp. 68-78, 2002.

[14] W.M. Huang, X.Y. Gao, B.K. Loo, L.M. He, and B.K.A. Ngoi, "Microgripper using two-way shape memory alloy thin sheet", Materials Science Forum, Vol. 394, No. 3, pp. 95-98, 2002.

[15] B. Sutapun and M. Huff, "Applications of shape memory alloys in optics", Applied Optics, Vol. 37, No. 28, pp. 6811-6815, 1998.

[16] I. Chopra, "Review of state of art of smart structures and integrated systems", American Institute of Aeronautics and Astronautics Journal, Vol. 40, No. 11, pp. 2145-2187, 2002.

[17] J.G. Boyd and D.C. Lagoudas, "A thermodynamical constitutive model for shape memory materials—Part I: The monolithic shape memory alloy", International Journal of Plasticity, Vol. 12, No. 7, pp. 805-842, 1996.

[18] M.H. Wu, "Fabrication of nitinol materials and components", Materials Science Forum, Vol. 394-395, pp. 285-292, 2002.

[19] M.A. Qidwai, A. Bhattacharyya, I. Vahhi, and S. Pulnev, "Initial investigation in actuator design using high-temperature shape memory alloy", Proceedings of SPIE—The International Society for Optical Engineering, Vol. 5053, pp. 81-91, 2003.

[20] S. Esteves, "CMOS micromachined devices for applications in fluids", M.Sc. thesis, University of Alberta, Canada, 2000.

[21] A. Bhattacharyya, L. Sweeney, and M.G. Faulkner, "Experimental characterization of free convection during thermal phase transformations in shape memory alloy wires", Smart Materials and Structures, Vol. 11, No. 3, pp. 411-422, 2002.

[22] M. Whitley, J.A. Hammer, Z. Hao, B. Wingfield, and L. Nelson, "A single two-axis micromachined tilt mirror and linear array", Proceedings of SPIE—The International Society for Optical Engineering, Vol. 4985, pp. 83-94, 2003.

Appendix: Proposed Two-Way Training Process of the SMA-Layered Cantilever

A schematic of a SMA-layered cantilever is depicted in Fig. 3. The cantilever can act as a mirror if it is coated with a reflective material. When an electric current (**I**) is passed through the SMA trace in the presence of an external magnetic field (**B**), the resulting Lorentz force (**F**) deflects the cantilever from its rest position. This nonintrusive approach of application of an external force coupled with heat treatment can lead to two-way training of the SMA-layered cantilever. A scenario of the SMA-actuated cantilever is now described using Fig. 4, where the vertical axis represents the expected predominantly compressive stress state in the SMA layer. Transformation temperatures of an SMA are highly sensitive to the alloy content. For our application, we will consider the SMA to have transformation temperatures that are all above the room temperature, T_0 (~25°C), i.e., $M_f > T_0$. It is then expected that the SMA will be in the martensitic state after the SMA-layered microcantilever has been fabricated. The training of the SMA-layered microcantilever can now proceed using a sequence of annealing first while in a deflected position using the Lorentz force, **F** (the loop *ABCD*). This is followed by repetitive thermal cooling and heating in the presence of the Lorentz force in the direction indicated in the figure (the loop *EFGH*). After this training procedure, the room-temperature martensitic "flat" state is expected to change to a high-temperature austenitic "deflected" state on heating (and vice versa). Thus, electrical heating of the SMA layer may be used to activate the two-way memory effect to bend the microcantilever. The cyclic increase and decrease in temperature due to electrical heating and subsequent cooling, respectively, will allow the SMA to switch between the austenite and martensite phases. Partial phase transformation by appropriate control of the thermal actuation will allow the microcantilever to take any position between the "rest" state and the fully actuated state. The modeling of the actuation of the SMA-layered cantilever will take the "two-way"–trained cantilever as its starting point and then determine the steady-state deflections of the cantilever when the SMA is heated.